

## Spider-silk inspired ultrafast alkali-induced molecular aggregation for 3D printing arbitrary tubular hydrogel

Yang Lyu<sup>a</sup>, Zhongying Ji<sup>a, b\*</sup>, Di Liu<sup>c</sup>, Xinqiang Xu<sup>d</sup>, Guo Rui<sup>a, b</sup>, Xinyan Shi<sup>c</sup>, Xiaolong Wang<sup>a, b\*</sup>

<sup>a</sup>Shandong Laboratory of Advanced Materials and Green Manufacturing at Yantai, Yantai Zhongke Research Institute of Advanced Materials and Green Chemical Engineering, Yantai, 264006, China

<sup>b</sup>State Key Laboratory of Solid Lubrication, Lanzhou Institute of Chemical Physics, Chinese Academy of Sciences, Lanzhou 730000, China

<sup>c</sup>Key Laboratory of Rubber-plastics, Ministry of Education, School of Polymer Science and Engineering, Qingdao University of Science & Technology, Qingdao, 266042, China

<sup>d</sup>School of Chemistry and Chemical Engineering, Key Laboratory of Materials-Oriented Chemical Engineering of Xinjiang Uygur Autonomous Region, Shihezi University, Shihezi, 832003, China.

## **Section 1. Materials and methods**

### **Materials**

All chemicals were used without further purification. Polyvinyl alcohol (PVA, lot number 30153160, molecular weight 75000 to 80000, 98% hydrolysis, Sinopharm Chemical Reagent Co., Ltd). 1-Butyl-3-methylimidazolium tetrafluoroborate (lot number A060002, molecular weight 226.03, Energy Chemical). 1-Butyl-3-methylimidazolium acetate (lot number XW2840497581, molecular weight 198.26, Energy Chemical). 1-Ethyl-1-methylpyrrolidinium bromide (lot number E1050, molecular weight 194.12, Energy Chemical). 1-Butylpyridinium hexafluorophosphate (lot number B2196, molecular weight 281.18, Energy Chemical). 1-Butylpyridinium bromide (lot number H26995, molecular weight 216.12, Energy Chemical). Sodium hydroxide (NaOH, lot number W810069, Energy Chemical). Potassium hydroxide (KOH, lot number 06055, Sigma-Aldrich). Barium hydroxide (lot number B50460, Acme biochemical). Carboxylated cellulose nanofibers (CNF, lot number C11118234, diameter 50nm, length 1-3 $\mu$ m, Macklin Reagent). Deionized (DI) water was made in the laboratory.

### **Preparation of PVA-OH hydrogels**

PVA and ILs was dissolved in distilled at 98 °C under stirring until the solution became homogeneous. Different solution of PVA/ILs was poured into a large plate, after gelation using a high concentration solution of NaOH to form PVA-OH hydrogels. The number in PVA-OHx represents the content of NaOH in PVA-OH hydrogels.

### **Preparation of NaOH/CNF Solution**

NaOH/CNF solution was prepared by dissolving CNF (1 wt%) in NaOH and deionized water at -15 °C for 1 h. According to most references, the method contributes to break the hydrogen bonds inside the CNF and prevents its aggregation. The remaining solution was stored in a refrigerator at -15 °C.

### **Preparation of PVA/ILs/CNF Solution**

The solution of PVA/ILs was firstly prepared by dissolving PVA powder and ILs in deionized water. The solution was heated in an oil bath at 98 °C with stirring for 1 h. Subsequently, the aqueous solution of CNF was added in PVA/ILs solution and stirred for another 1h at room temperature.

### **Rheological characterization**

The rheological behavior of hydrogel ink and other individual components solutions was investigated by the rheometer (ARES-G2, TA Instruments) with a coaxial two parallel plate model, in which the clamp diameter is 25mm and the gap is 1mm. The plate temperature was set from 70 °C to 90 °C, and the frequency was from 10<sup>-2</sup> Hz to 10<sup>2</sup> Hz. Storage ( $G'$ ) and loss moduli ( $G''$ ) were probed via frequency test at  $\gamma = 0.1\%$  strain amplitude that lie in the linear viscoelastic region. By

following the principle of time-temperature superposition, master curves of  $G'$  and  $G''$  over a wide frequency range were constructed at a reference temperature of 80 °C.

#### **Mechanical property determination**

At least five dumbbell-shaped specimens were used for all tensile strength tests on the test machine (Z030, Zwick/Roell) at a strain rate of 50 mm/min. The stress-strain curves were measured by using the specimens (length  $\times$  width  $\times$  thickness of work region is 25 mm  $\times$  4 mm  $\times$  2 mm) at room temperature. The stress was evaluated by dividing the force by the initial cross-sectional area of the specimens, and the strain was evaluated by dividing the deformed length by the initial length. In addition, the area under the stress-strain curves was integrated to characterize the toughness. A cylindrical specimen (29 mm D  $\times$  12.5 mm H) was used for a typical compressive test on the same test machine at a compressive rate of 30 mm/min.

#### **Morphology Characterization**

All hydrogel specimens were frozen-drying using a SCIENTZ-10N/A freeze-dryer (Ningbo Scientz Biotechnology co., Ltd.) for characterization of the microstructure of the PCI hydrogels. The freeze-dried hydrogels were sputtered with gold after brittle fracture. Subsequently, the specimens were carried out imaging using a CLARA GHM SEM (TESCAN).

#### **X-ray Characterization**

All hydrogel specimens were performed on XRD (D8 Focus, Bruker) to compare the crystallinity by Cu-K $\alpha$  radiation in a  $2\theta$  range of 10° to 50°. The scan speed was 3°/min.

#### **Thermal properties characterization**

The thermal properties of PVA-OH were investigated using a differential scanning calorimeter (DSC) (DSC 204F1, NETZSCH instruments, Germany). To prepare samples for DSC, the dried samples were weighed (between 5-10 mg) in standard aluminum pans, sealed with lids, heated at the rate of 20 °C/min from 25 to 230 °C using nitrogen as a purge gas.

#### **Chemical properties characterization**

The chemical structure of PVA-OH were analyzed with proton nuclear magnetic resonance ( $^1\text{H}$ NMR) spectroscopy, and Fourier transformed infrared (FTIR). FTIR spectroscopy (VERTEX70, Bruker, Germany) was performed using the attenuated total reflectance (ATR) mode in the range of 400-4000  $\text{cm}^{-1}$ .

Section 2. Figure S1 to S13

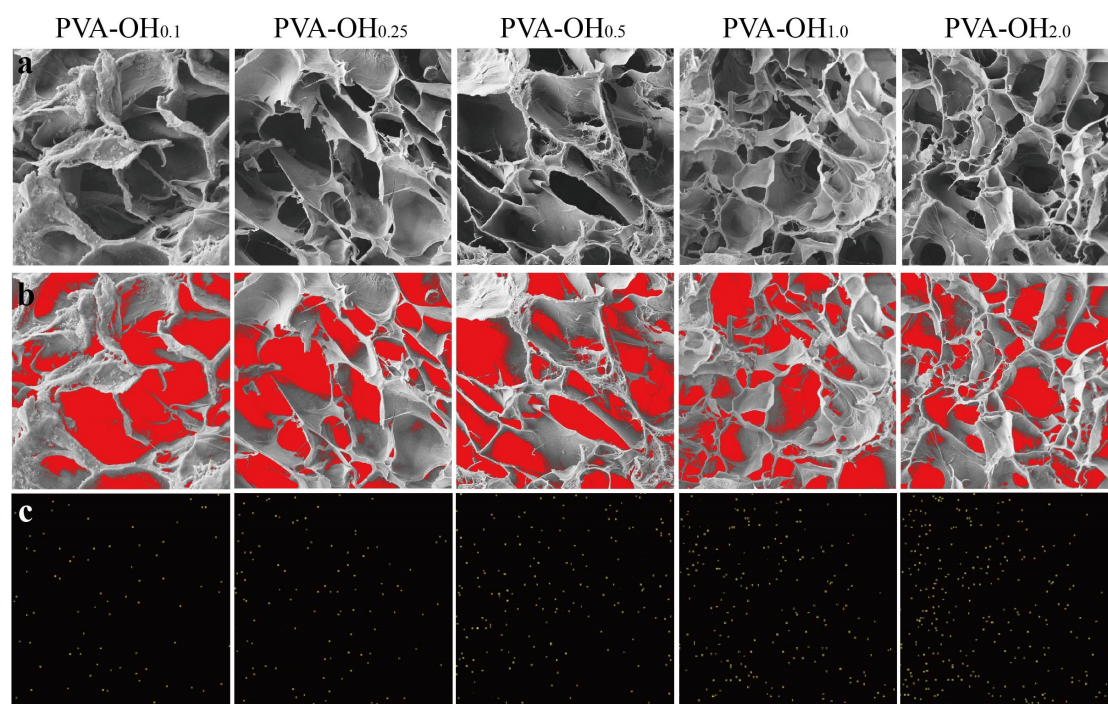


Fig.S1 Porosity images of PVA-OH hydrogel samples with different alkali concentrations calculated by Image J software. Detection of [BMIM]BF<sub>4</sub> distribution in PVA-OH hydrogel samples by energy dispersive spectrometer (EDS) analysis of F element.

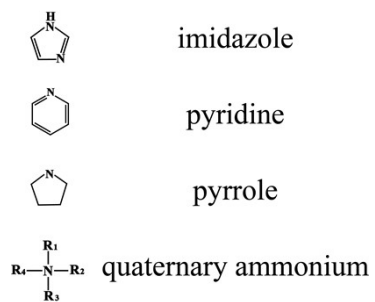


Fig.S2 The structural formula of cations used in Fig.2j and k.

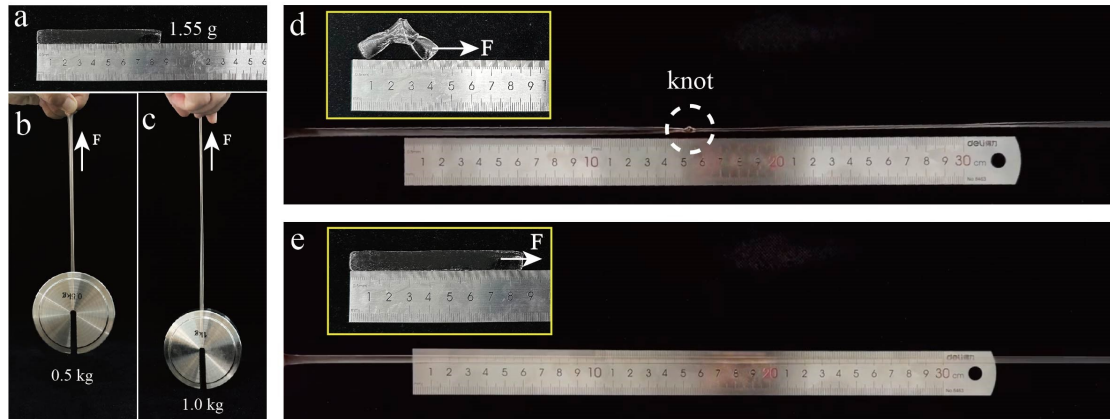


Fig.S3 Photos of mechanical properties of PVA-OH<sub>2.0</sub> hydrogel samples (All samples are treated by freeze-thaw cycles). (a) The original length and weight of the sample is 8.5cm and 1.55g, respectively. The PVA-OH<sub>2.0</sub> hydrogel sample can lift 0.5kg (b) and 1.0kg (c) dumbbells. The PVA-OH<sub>2.0</sub> hydrogel sample can be stretched over 5 times longer than the original length with (d) or without (e) a knot.

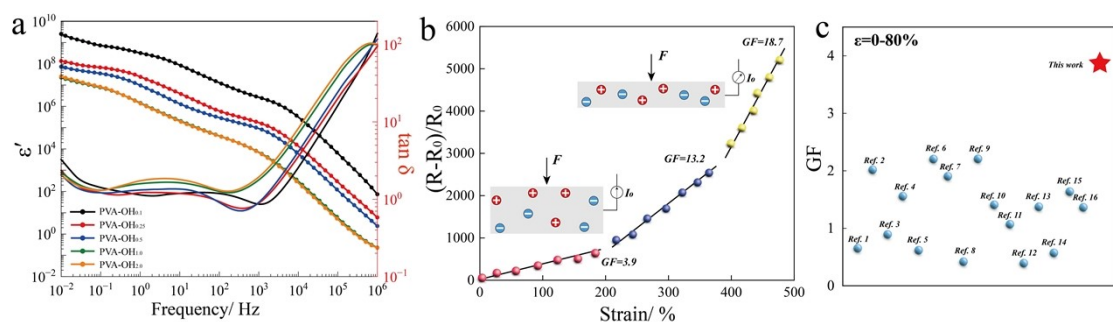


Fig.S4 (a) The frequency dependence of the dielectric constant and dielectric loss. (b) Ashby charts of the Sensitivity of PVA-OH sensors versus various other PVA-based hydrogels. (c) Comparison of sensitivity at 80% strain with flexible strain sensors reported.

Ionic liquids in systems endow PVA-OH hydrogels with great conductivity, permit vessel models to have more novel functions. The variations of real ( $\epsilon'$ ) dielectric constants and dielectric loss ( $\tan \delta = \epsilon''/\epsilon'$ ) in hydrogels with respect to the frequency are governed by the intrinsic polarization of interaction. It is evident that the  $\epsilon'$  of PVA-OH hydrogels decreased gradually with increasing the content of NaOH over the test frequency, which is primarily ascribed to the enhanced complexation restrains the accumulation of charges and reduces the intrinsic polarization (*Fig.S4a*). The sensitivity of the sensor represented by the relationship between the relative resistance change and the tensile strain of the PVA-OH hydrogel (*Fig.S4b*). The ratio of the two is defined as the gauge factor (GF) to characterize the sensitivity of its tensile strain sensing. It can be observed that the sensitivity exhibits piecewise linear characteristics. The GF changed from 3.9 (0-200%) to 13.2 (200-400%) and finally reached 18.7 with large strains (400-500%). The excellent sensitivity ensures a clear electrical signal response even at low strains. Compared with previous literature, the GF of PVA-OH hydrogel is significantly higher than others at 80% strain (*Fig.S4c*) [1-16].

## Reference

- [1] Xintong Hu, Jianhua Wang, Shiqiang Song, et al. Ionic Conductive Konjac Glucomannan/Liquid Crystal Cellulose Composite Hydrogels with Dual Sensing of Photo- and Electro-Signals Capacities as Wearable Strain Sensors. *International Journal of Biological Macromolecules*. 2024, 258(2): 129038.
- [2] Xi Zhang, Xiangli Kong, Xin Zhou, et al. Antimicrobial and Anti-freezing Conductive Hydrogels Driven by Quaternary Ammonium Chitosan Salt for Flexible Strain Sensors. *European Polymer Journal*. 2024, 202: 112601.
- [3] Huijuan Lin, Wenlong Yuan, Hong Shao, et al. Muscle-inspired Anisotropic Hydrogel Strain Sensors with Ultra-strong Mechanical Properties and Improved Sensing Capabilities for Human Motion Detection and Morse Code Transmission. *European Polymer Journal*. 2024, 202: 112642.
- [4] Daiwei Chen, Huiyu Bai, Haiyan Zhu, et al. Anti-freezing, Tough, and Stretchable Ionic Conductive Hydrogel with Multi-crosslinked Double-network For A Flexible Strain Sensor.

- Chemical Engineering Journal. 2024, 480: 148192.
- [5] Juan Wang, Peng Du, Yu I Hsu, et al. Rapid Preparation of Dynamic-crosslinked Nanocomposite Hydrogel Sensors with Efficiency Self-healing and Adhesion Properties for Elderly Health and Sleep Management. Chemical Engineering Journal. 2024, 480: 148324.
- [6] Yibo Sun, Zhe Yu, Yiyan Gao, et al. Flexible Hydrogel Sensor with Excellent Antibacterial and Low Temperature Frost Resistance. Polymer. 2023, 283: 126282.
- [7] Feiyue Hao, Shuang Sun, Yizhe Xu, et al. 3D Printing of Flexible Sensors Based on Polyvinyl Alcohol/carboxylated Chitosan/sodium Alginate/silver Nanowire High-strength Hydrogels. Polymer. 2024, 290: 126594.
- [8] Qiuyu Xu, Mohan Hou, Lifang Wang, et al. Anti-bacterial, Anti-freezing Starch/ionic liquid/PVA Ion-conductive Hydrogel with High Performance for Multi-stimulation Sensitive Responsive Sensors. Chemical Engineering Journal. 2023, 477: 147065.
- [9] Rujun Dai, Yiyan Gao, Yibo Sun, et al. Ionic Conductive Amylopectin Hydrogels for Biocompatible and Anti-freezing Wearable Sensors. European Polymer Journal. 2023, 200: 112496.
- [10] Haihua Wang, Leixin Meng, Yanan Ye, et al. Antibacterial Zwitterionic Hydrogel for Flexible and Wearable Ultrafast-Response Strain Sensors with Low Hysteresis. 2024, 17: 100234.
- [11] Jie Zhang, Yong Li, Jiana Pan, et al. Silk Fibroin Enhanced Double-network Hydrogels with Extreme Stretchability, Self-adhesive and Biocompatibility for Ultrasensitive Strain Sensors. Colloids and Surfaces A: Physicochemical and Engineering Aspects. 2024, 684: 133035.
- [12] Xiangrui Yan, Rongrong Zhao, Huijuan Lin, et al. Dual-network Conductive Hydrogel with Rapid Self-healing Ability and Great Fatigue Resistance as Strain Sensor for Human Motion Monitoring. European Polymer Journal. 2023, 201: 112570.
- [13] Shuyu Wang, Shuaiyang Duan, Tianyu Yang, et al. A Self-powered Strain Sensor Utilizing Hydrogel-nanosheet Composites, Zn Foil, and Silver-coated Nylon. Sensors and Actuators: A. Physical. 2023, 364: 114824.
- [14] Bengang Li, Yurui Chen, Wei Wu, et al. Copolymer-grafted Cellulose Nanocrystal Induced Nanocomposite Hydrogels with Enhanced Strength, High Elasticity and Adhesiveness for Flexible Strain and Pressure Sensors. Carbohydrate Polymers. 2023, 317: 121092.
- [15] Yingjie Wang, Linneng Song, Qi Wang, et al. Multifunctional Acetylated Distarch Phosphate Based Conducting Hydrogel with High Stretchability, Ultralow Hysteresis and Fast Response for Wearable Strain Sensors. Carbohydrate Polymers. 2023, 318: 121106.
- [16] Yinjie Peng, Shiqing Tang, Xiaoyu Wang, et al. A High Strength Hydrogel with a Core-Shell Structure Simultaneously Serving as Strain Sensor and Solar Water Evaporator. Macromolecular Materials and Engineering. 2021, 306(10): 2100309.



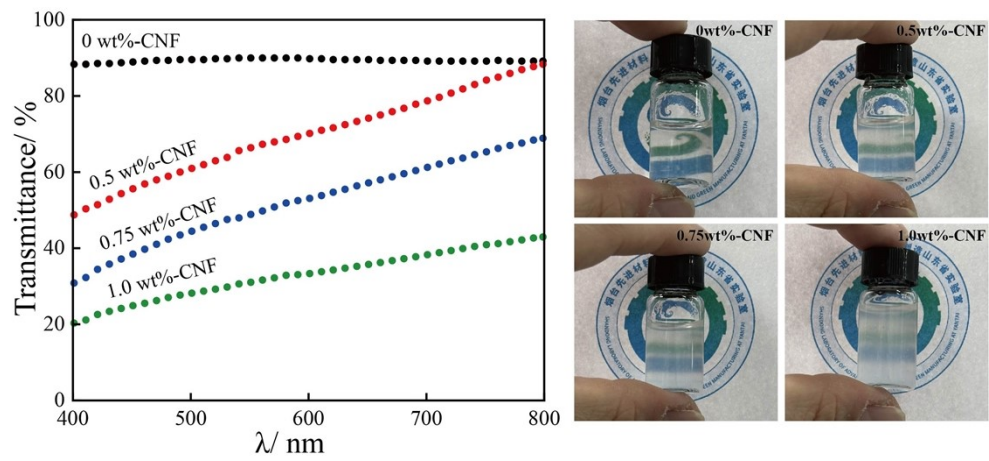


Fig.S5 The transparency of PVA/ILs medium with different content of CNF

The transparency of PVA/ILs medium reduced gradually with the increase of CNF content.

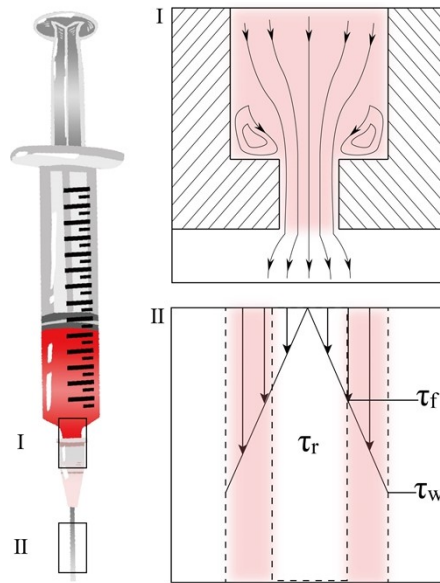


Fig.S6 Schematic diagram of shear force with alkali/CNF solution flowing through the micro needle

As the tip moves, the NaOH/CNF locally fluidizes and then rapidly solidifies, leaving a drawn cylinder in its wake. Subsequently, NaOH diffuses into PVA/[BMIM]BF<sub>4</sub>/CNF gel medium, solidifies and forms a cavity.

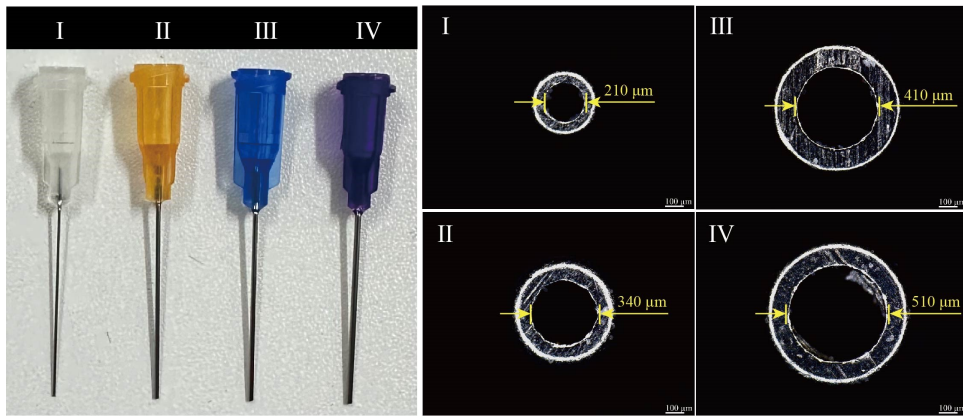


Fig.S7 Photos of four micro needle with different diameter.

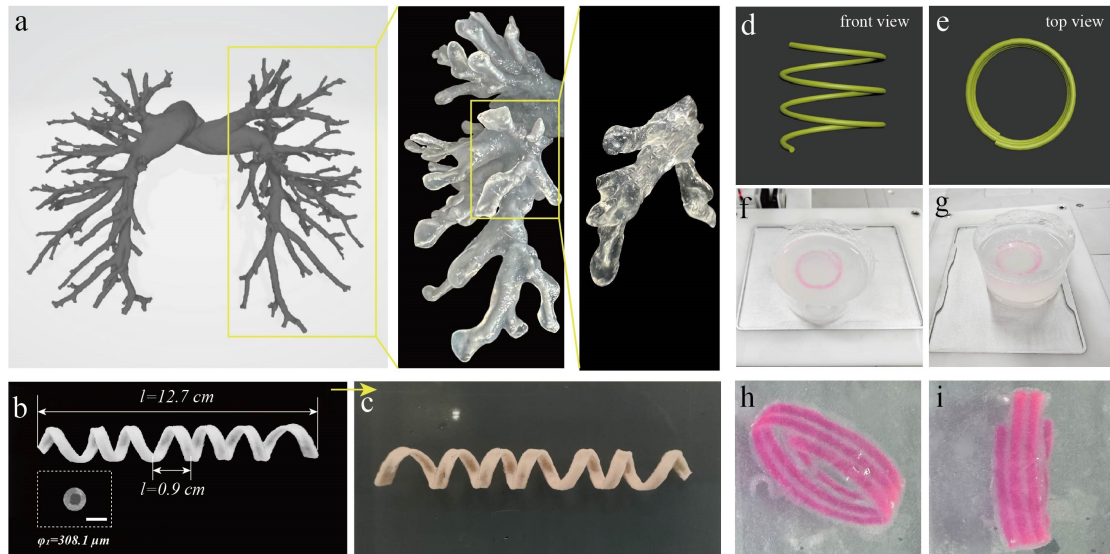


Fig.S8 Photos of various 3D hollow hydrogel structures fabricated by this strategy. (a) A hollow hydrogel structure with the shape of pulmonary vessels and its enlarged image (b) 3D printing hydrogel spiral tube with the diameter of 308.1  $\mu\text{m}$  and the length of 12.7 cm. (c) Injected orange liquid into the hydrogel spiral tube. (d) Front view and (e) top view of 3D model of spiral lines with large diameter. (f-g) Photos of spiral tubes by 3D printed in PVA/[BMIM]BF<sub>4</sub>/CNF gel medium. The stain was added in injected material (alkali/CNF) to distinguish from the medium. (h-i) Photos of hollow spiral tubes fabricated by this strategy.

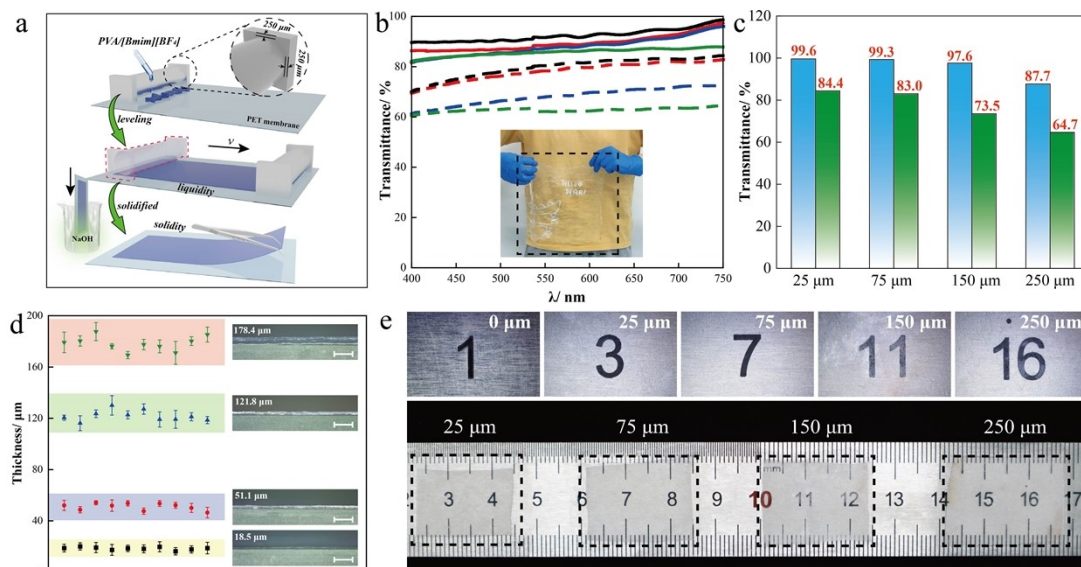


Fig.S9 Fabricate ultrathin hydrogel membranes by doctor-blade method. (a) Schematic representation of fabricating ultrathin hydrogel membranes with different doctor blade. (b) Transparency of ultrathin hydrogel membranes. The dashed and solid lines indicate the samples with or without freeze-thaw cycles, respectively. (c) Transparency of ultrathin hydrogel membranes prepared with different thickness of doctor blade. The green and blue columns indicate the samples with or without freeze-thaw cycles, respectively. (d) Four thicknesses of hydrogel membranes prepared by four thicknesses of doctor blades (25, 75, 150 and 250  $\mu\text{m}$ ). Each sample was prepared ten times by the same method to reduce errors. (e) Photos of transparency of ultrathin hydrogel membranes with different thicknesses.

Schematic of the membrane applicator used in this work is shown in Fig.S9a. It works on the principle of doctor blade coating technique to yield uniform thin membranes of the PVA/[BMIM]BF<sub>4</sub> solution onto the substrate (polyethylene terephthalate, PET film with thickness of 0.5 mm). The thickness of hydrogel membranes was controlled by different doctor blade fitted with an adjustable micrometer scale to adjust the height of the blade (from 25 to 250  $\mu\text{m}$ ) and the speed of the doctor blade is 20 mm/s. Then both PET film and PVA/[BMIM]BF<sub>4</sub> solution was immersed into NaOH (2.0 mol/L) to solidify and obtain an ultrathin hydrogel membrane.

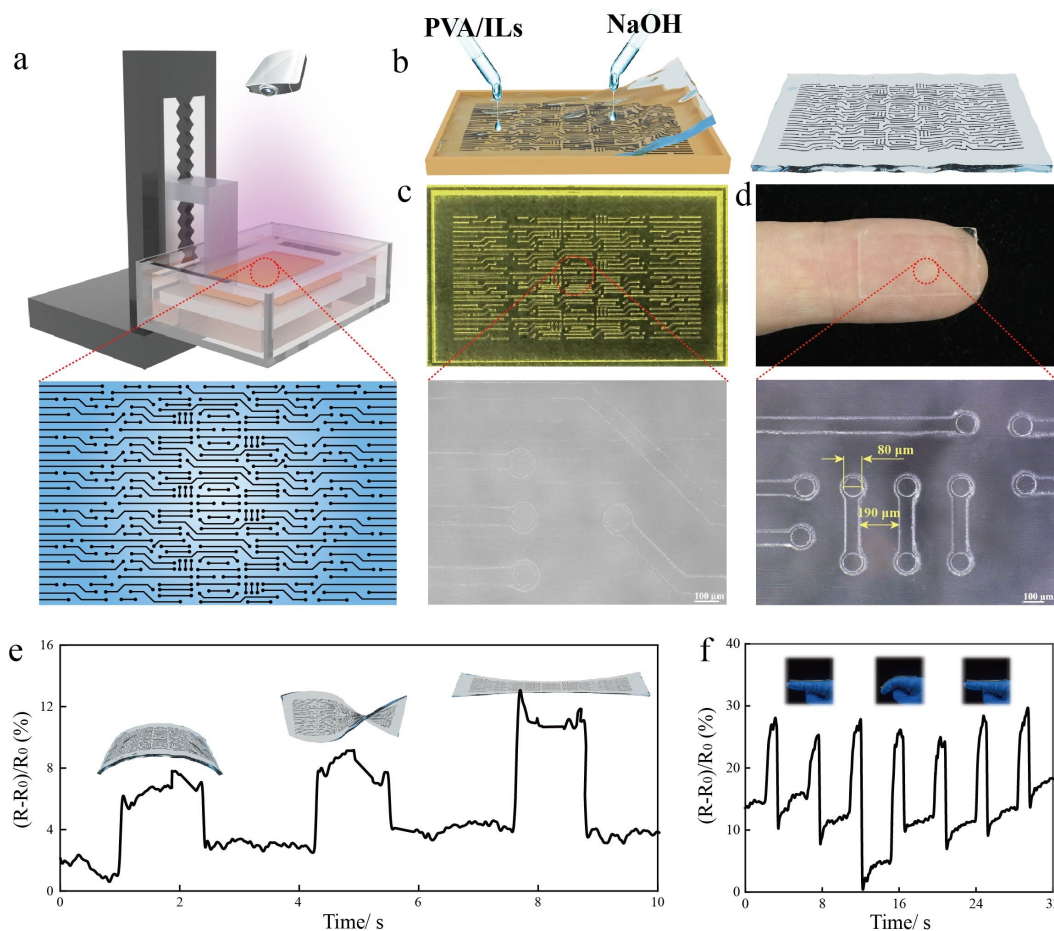


Fig.S10 Illustration of the fabrication process of hydrogel sensors with refined structure and properties. (a-b) Preparation of precision structure hydrogels by stereo lithography appearance (SLA) and template method. (c) Photo of a negative circuit board template by 3D printed. (d) The positive hydrogel replica and SEM image. (e) Electrical signals of hydrogel sensors (15 mm L  $\times$  10 mm W  $\times$  0.8 mm H) under the shape changes of bending, twisting and stretching. (f) Hydrogel sensor was attached to fingers and detected the electric signals of finger bending.

A resin circuit model was first prepared by SLA 3D printing. Subsequently, the pre-rinsed resin circuit model was used as the negative template which then coating PVA/[BMIM]BF<sub>4</sub> and NaOH solution sequentially to fabricate the positive hydrogel replica. The positive hydrogel replica can be peeled conveniently due to no interaction between hydrogel and resin.

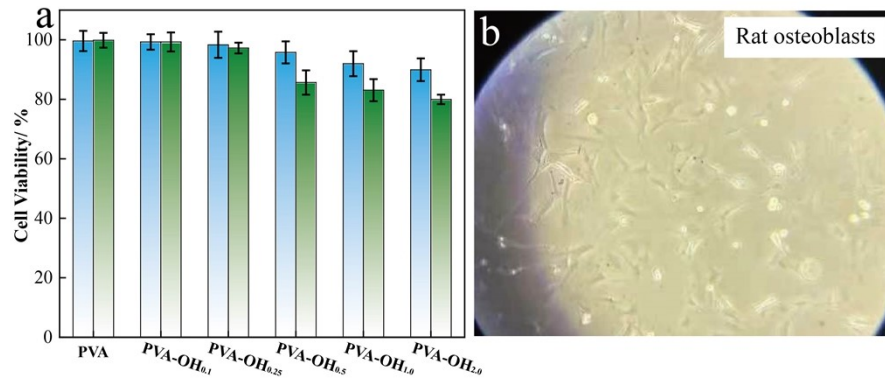


Fig.S11 (a) Cell survival rate of leaching solution of different hydrogel samples. (b) Photo of rat osteoblasts used in this section.


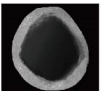

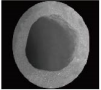

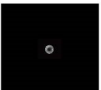
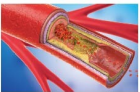
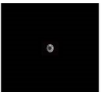
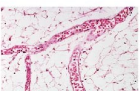

organ	mean diameter	mean wall thickness	sketch	hydrogel	parameter
Artery	4.0 mm	1.0 mm			d=0.51 mm c(OH <sup>-</sup> )=2.0 mol/L Δp=0.14 MPa v=12 mm/s
Vein	5.0 mm	0.5 mm			d=0.51 mm c(OH <sup>-</sup> )=1.0 mol/L Δp=0.14 MPa v=10 mm/s
Arteriole	30 μm	6.0 μm			d=0.06 mm c(OH <sup>-</sup> )=1.0 mol/L Δp=0.08 MPa v=10 mm/s
Venule	20 μm	1.0 μm			d=0.06 mm c(OH <sup>-</sup> )=1.0 mol/L Δp=0.08 MPa v=10 mm/s
Capillary	8.0 μm	0.5 μm			d=0.04 mm c(OH <sup>-</sup> )=0.5 mol/L Δp=0.06 MPa v=10 mm/s

Fig.S12 The diameter of vessels of different organs and fabricating parameters of hydrogel tubes with similar structures.

Hydrogel vessels fabricated by this strategy can be used as the in vitro realistic hands-on platform for simulating the endovascular intervention, overcoming those issues including the lack of spatial information in X-ray angiography for diagnosis and treatment, the inappropriate choice of medical devices caused side effect, and the limited nonliving training platforms.



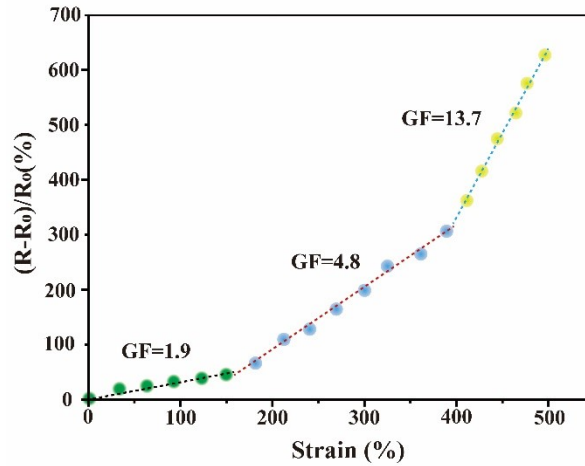


Fig. R13 Relative resistance variation of the conductive hydrogel upon stretching  
 The gauge factor (GF) [1-3] is a crucial indicator of the hydrogel's resistance change with strain, representing the sensitivity of the relationship between resistance and strain in the hydrogel. The sensitivity of hydrogel sensors progresses through three stages as strain levels increase. GF values are 1.9 for strains below 150%, 4.8 between 150% and 400%, and 13.7 between 400% and 500%. Consequently, the sensitivity of PVA hydrogel flexible sensors improves with higher strain levels.

[1] Guo B, Zhong Y, Chen X, et al. 3D printing of electrically conductive and degradable hydrogel for epidermal strain sensor [J]. *Composites Communications*, 2023, 37: 101454.

[2] Liao XQ, Liao QL, Yan XQ, et al. Flexible and Highly Sensitive Strain Sensors Fabricated by Pencil Drawn for Wearable Monitor [J]. *Advanced Functional Materials*. 2015, 25, 2395-2401.

[3] Ma SS, Xue P, Valenzuela C, et al. Flexible and Highly Sensitive Strain Sensors Fabricated by Pencil Drawn for Wearable Monitor [J]. *Advanced Functional Materials*. 2024, 34, 2309899.

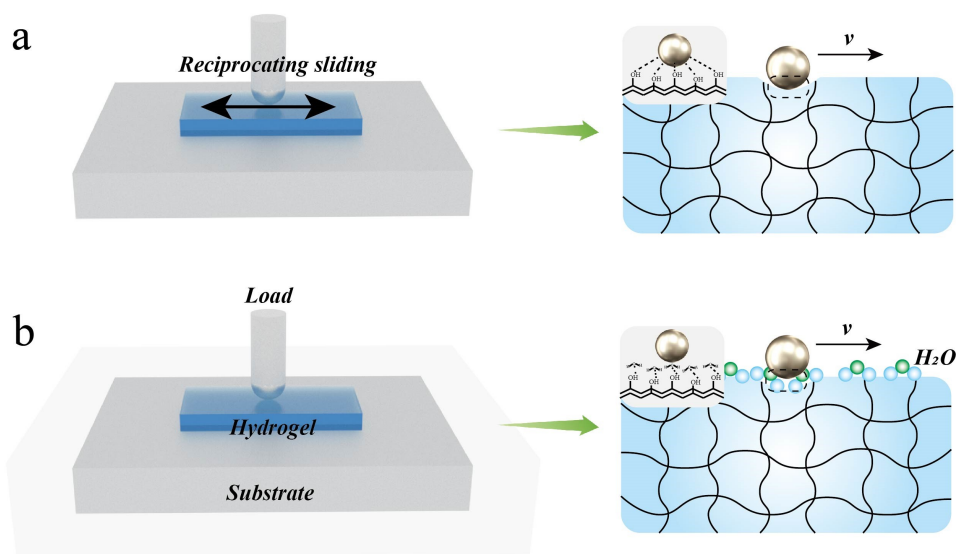


Fig.S14 The schematic illustration of the friction process without (a) and with (b) water. Fig.S13 illustrates a schematic diagram of the friction testing process of PVA-OH hydrogels, and the average coefficient of friction (COF) was collected by employing a ball-on-disk tribometer with a reciprocating sliding contact mode in (or no) water lubricants. Each measurement was performed with 300 sliding cycles at a fixed frequency of 1 Hz.